Journal of Materials Chemistry C

PAPER

View Article Online
View Journal

Cite this: DOI: 10.1039/c7tc02528a

Orthogonal 4,10 and 6,12 substitution of dibenzo[def,mno]chrysene polycyclic aromatic small molecules†

Unsal Koldemir,‡[a] Jonathan S. Tinkham,[a] Robert Johnson,[ab] Bogyu Lim,[c] Henok A. Yemam,[a] Kevin J. Gagnon,[d] Sean Parkin[e] and Alan Sellinger*[af]

Received 7th June 2017,
Accepted 29th June 2017

DOI: 10.1039/c7tc02528a

rsc.li/materials-c

A series of new polycyclic aromatic hydrocarbon compounds based on (4,10-disubstituted-dibenzo-[def,mno]chrysene-6,12-dione) and 4,10 di-substituted 6,12-bis(triisopropylsilylethynyl)dibenzo[def,mno]-chrysene are reported with tunable electronic properties through varied molecular architecture. Starting with an inexpensive commercially available textile dye known as Vat Orange #3, (4,10-dibromo-dibenzo[def,mno] chrysene-6,12-dione) we extended the conjugation at the 4- and 10-positions by the attachment of both electron rich and deficient hexylvinylphthalimide, thiophene, hexylthiophene, triphenylamine, and hexylbithiophene aromatic groups, and studied the resultant optoelectronic properties. By applying various synthetic metal-catalyzed reactions, soluble dibenzo[def,mno]chrysene and dibenzo[def,mno]chrysene-6,12-dione derivatives were achieved with optical edge band gaps between 2.30 eV and 1.65 eV.

Introduction

Conjugated aromatics, whether small- or macromolecular, have been active materials of choice as soft semiconductor materials for organic electronic applications such as organic photovoltaics (OPV), organic field effect transistors (OFET) or organic light emitting diodes (OLED).[1–5] Compared to conjugated polymers, small-molecule organic systems have gained attention as they provide simpler syntheses and higher degrees of purity that can be obtained *via* recrystallization, sublimation, and/or chromatographic methods.[6] They also offer the ability to be processed into devices *via* solution or *via* vacuum deposition, the latter of which is not feasible for macromolecular conjugated polymers.[7,8] As such, a large variety of polycyclic aromatic hydrocarbon (PAH) based small-molecule systems have gained widespread interest due to their high charge-carrier mobilities and low lying HOMO energy levels.[9,10] One of the classes of such PAHs are the angular acenes, that feature non-linear extension of the acene skeleton. Theoretical studies have shown the angular extension of the acene skeleton increases the aromatic stabilization energy of the molecule, as opposed to the linear acenes where the gain in stabilization decreases with size,[11] as does their stability.[9,12] Linear acenes are able to form favorable interfacial dipole moments when coordinating to fullerenes,[13] but their instability causes a Diels–Alder reaction with fullerenes to occur, forming mono- and bis-adducts.[14,15] However, the increased stability of the angular acenes prevents formation of fullerene adducts,[15] that has been demonstrated experimentally between various dibenzochrysene isomers and [6,6]-phenyl-C_{61}-butyric acid methyl ester (PCBM) *via* ^{1}H NMR spectroscopy, with no reaction observed after several days.[16] The promise of the ideal properties of linear acenes with the stability of angular acenes has resulted in increased attention.[16–21]

To date, there have been reports on the optoelectronic properties of various DBC isomers and their utilization in organic electronic applications.[22–27] Small-molecule based bulk heterojunction (BHJ) organic solar cells employing soluble derivatives of dibenzochrysene as active donor material were reported to achieve power conversion efficiencies (PCEs) of 2.2% with a high open-circuit voltage (V_{oc}) of 0.91 V for dibenzo[*b*,def]chrysene and 1.95% with a V_{oc} of 0.80 V for the dibenzo[def,mno]chrysene analogues.[20,21] It is noteworthy that these molecules resulted in high V_{oc} due to their low lying HOMOs that is crucial for high performance organic photovoltaics. Our group has previously

[a] Department of Chemistry, Colorado School of Mines, Golden, CO 80401, USA. E-mail: aselli@mines.edu
[b] Departments of Chemistry, and Chemical and Biomolecular Engineering, North Carolina State University, Raleigh, NC 27695, USA
[c] Department of Materials Science and Engineering, Stanford University, Stanford, CA 90305, USA
[d] Advanced Light Source, LBNL, Berkeley, CA, 94720, USA
[e] Department of Chemistry, University of Kentucky, Lexington, KY 40506, USA
[f] Materials Science Program, Colorado School of Mines, Golden, CO 80401, USA

† Electronic supplementary information (ESI) available. CCDC 1526927 and 1526928. For ESI and crystallographic data in CIF or other electronic format see DOI: 10.1039/c7tc02528a

‡ Contributed equally to this work.

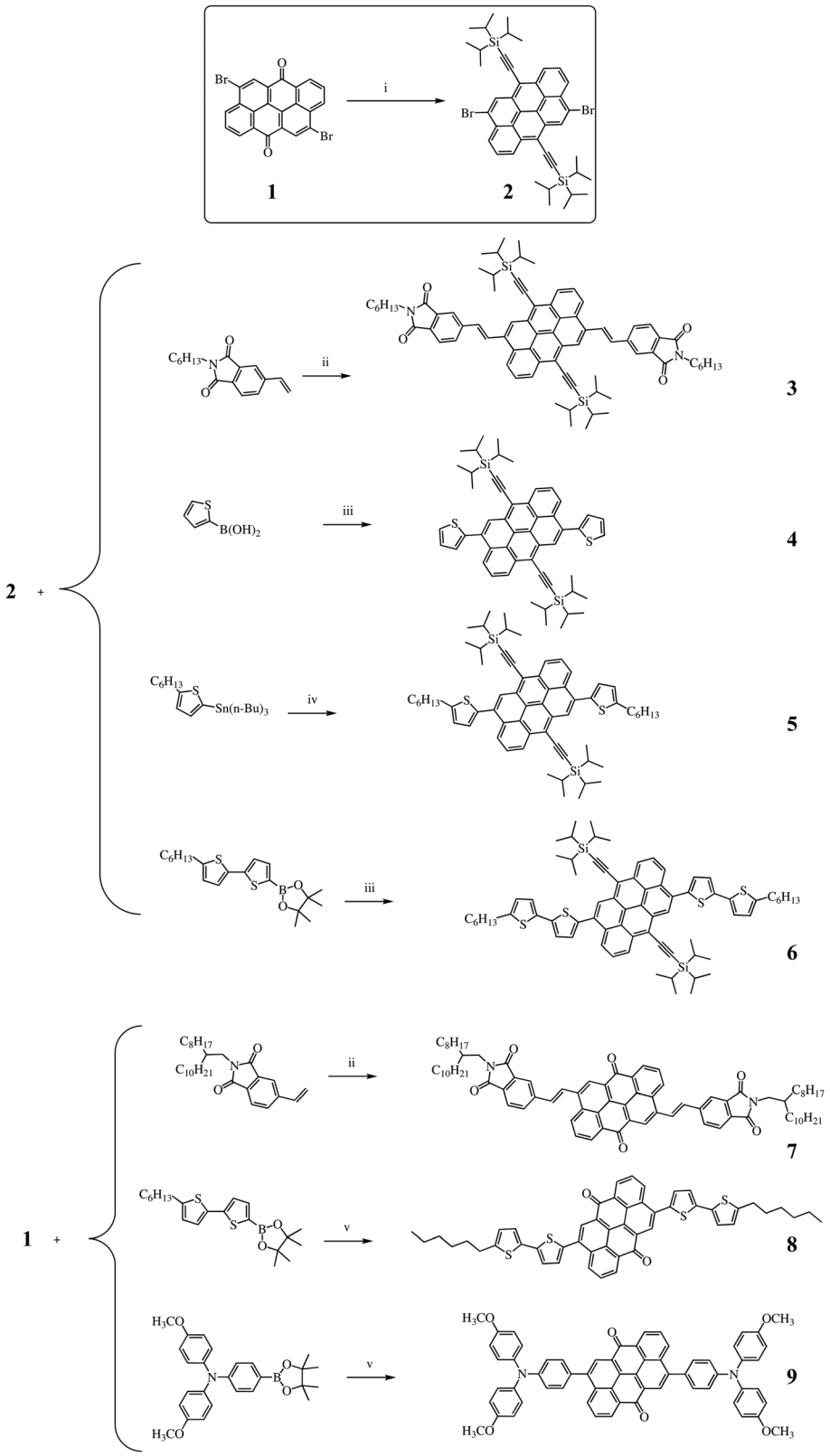

Scheme 1 The synthetic pathway to the derivatives: (i) (triisopropylsilyl)acetylene/*n*-butyl lithium; 3 M HCl $SnCl_2{\cdot}2H_2O$ (ii) $Pd(tBu_3P)_2$, NCy_2Me, PhMe. (iii) Aliquat 336, K_2CO_3, $Pd(PPh_3)_4$, PhMe. (iv) $Pd(PPh_3)_4$, PhMe. (v) Aliquat 336, CsF, $Pd(tBu_3P)_2$, THF : H_2O (15 : 1).

reported chromophore-flanked, pyrene-core, star-shaped small molecules prepared in order to achieve extended and delocalized π-electron aromatic systems with potential application in organic light-emitting diodes (OLEDs).[28] In particular,

dibenzo[def,mno]chrysene (DBC) is of interest due to the extension of the skeleton relative to pyrene, but also the availability of an inexpensive precursor dye: 4,10-dibromo-dibenzo[def,mno]chrysene-6,12-dione (DBC-DO) (known as Vat Orange 3). The 6,12-location of the ketones allows orthogonal functionalization relative to the 4,10-bromo groups, and this allows the study of substitution at each position, and their influence on opto-electronic and solid-state behavior. In this report, we introduce DBC and DBC-DO derivatives based on the 6,12-dione and 6,12-di(triisopropylsilylacetylene) flanked at the 4,10 positions with vinylphthalimide, thiophene, and triarylamine moieties. Addition of the triisopropylsilyl group was selected due to the tendency of these groups to result in soluble and highly stackable molecules with unique molecular arrangements and large effects on bulk behavior,[17–19,29] while the dione is very electron withdrawing so as to introduce donor–acceptor (D–A) properties.

Using nucleophilic reduction chemistry on the 6,12-positions, while using palladium catalyzed cross-coupling reactions on the 4- and 10-positions we achieved soluble derivatives and studied their optoelectronic properties as well as crystal structures of a select few.

Results and discussion

The chemical structures and synthesis of the new derivatives **3–9** are given in Scheme 1. Starting from the commercially available textile dye Vat Orange 3 (**1**), we installed triisopropylsilylacetylene groups *via* reductive substitution similar to procedures reported previously.[21,22,24] Basically compound **1** (Vat Orange 3, 4,10-dibromo-dibenzo[def,mno]chrysene-6,12-dione) was reacted with *in situ* prepared lithium triisopropylsilylacetylide and then treated with $SnCl_2$ in 3 M HCl to promote reduction resulting in the desired compound **2** through dehydration and aromatization steps.[22] Next, palladium-catalyzed Heck, Stille and Suzuki–Miyaura couplings were utilized to flank both the starting material **1** and compound **2** with vinyl-*N*-hexylphthalimide, thiophene, hexylthiophene, hexylbithiophene, and triarylamine affording the new DBC and DBC-DO derivatives. The DBC based compounds were purified *via* flash-chromatography over silica gel to afford dark-colored solids with yields of 59–75%. The DBC-DO compounds were purified in a similar manner, but the insolubility of **1** in DCM allowed the product to be purified by trituration in DCM followed by dissolution in $CHCl_3$ and precipitation in acidic methanol, yielding compounds **7–9** as dark-colored powders. These compounds were soluble in common organic solvents such as DCM, THF, chloroform, and toluene at room temperature. Structural composition of these molecules was confirmed with ^{1}H-NMR spectroscopy, in which the expected aromatic and aliphatic proton singles were observed (Fig. S8–S14, ESI†). We attempted structural characterization with ^{13}C NMR, however, the aromatic carbon peaks were not discernible. MALDI-MS with 1,8,9-trihydroxyanthracene as the matrix analysis revealed the molecular mass ion [M^+] peak for each compound were consistent with their theoretical masses (Fig. S1–S7, ESI†). An example MALDI-MS in shown in Fig. 1 for compound **3**. The lower MW peaks are likely due to fragmentation during the MALDI ionization experiment.

Compound **8** was not soluble in DCM, and was collected as a precipitate and purified by washing with MeOH and DCM, before being redissolved in $CHCl_3$ and collected. The structure for **8** was confirmed by MALDI, but obtaining a clear ^{1}H NMR required addition of trifluoroacetic acid to further solubilize the compound.

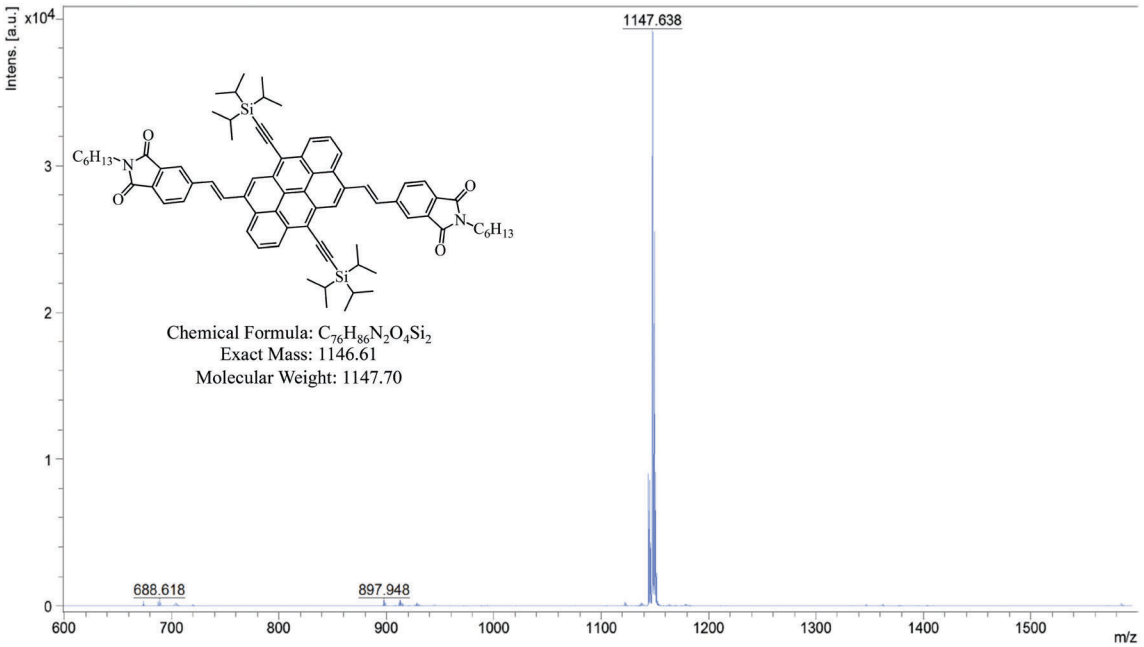

Fig. 1 MALDI spectrum of compound **3**.

Optical properties

Absorption properties of the products were studied with UV-Vis spectroscopy both in dilute DCM solution and in thin films drop-cast from DCM solutions onto glass substrates. The resulting thin-film spectra are shown in Fig. 2 and summarized in Table 1 (solution-phase spectra in Fig. S16, ESI†). For compounds **4–6**, and **8–9**, there is a negligible bathochromic shift of 5–8 nm in the λ_{max} between the solution and thin-film spectra, accompanied by a slight broadening of the thin-film spectra. Compounds **3** and **7**, the vinylphthalimide derivatives, showed a larger 12 nm hypsochromic shift along with a more appreciable broadening compared to its solution spectrum, indicative of increased intermolecular interactions in the solid state.[21]

Compounds **4–6** differ little in their optical bandgap, which is unexpected given the increased conjugation expected for compound **6** relative to **4** and **5**. This is indicative of little electronic communication between the core and peripheral thiophenes. Compound **3** has a slight reduction in bandgap, expected from the withdrawing nature of the phthalimide group, but this appears to be more a result of increased broadening of its peak. Similarly, compounds **7** and **8** show a much smaller difference in optical bandgap than expected, given the difference in electronic strength of the attached unit.

Compound **9** has the smallest bandgap, despite the phenyl spacer. However, this is possibly due to a π–π* intramolecular charge-transfer (ICT) transition with the amine center, that is confirmed by computational modeling, as discussed later. In general, the optoelectronic properties of the DBC and DBC-DO cores have the largest effect on optical properties in solution and solid state, with only slight changes for each 6,10-substitution.

Thermal analysis on compounds **3–9** was performed using differential scanning calorimetry (DSC) (Fig. S18, ESI†) under a nitrogen atmosphere. Compounds **4–6** displayed weak thermal events assigned to being either glass (T_g) or melting (T_m) transitions. Compounds **3**, **7–9** did not display any thermal transitions.

Table 1 Optical and electrochemical characteristics of **3–9** as dropcast films

Compound	λ_{max} (nm)	λ_{onset} (nm)	E_g^{opt} (eV)	E_{HOMO}^{CV} (eV)	E_{LUMO}^{CV} (eV)	E_g^{CV} (eV)
3	346, 494	562	2.21	−5.40	−3.52	1.88
4	341, 471, 502	538	2.30	−5.38	−3.59	1.79
5	328, 474, 505	558	2.22	−5.44	−3.30	2.14
6	341, 479, 510	558	2.22	−5.44	−3.40	2.04
7	378, 537	643	1.93	−5.55	−3.94	1.61
8	330, 564	700	1.77	−5.50	−3.43	2.07
9	613	752	1.65	−5.07	−3.82	1.25

λ_{max} – wavelength at peak absorption. λ_{onset} – onset of absorption. E_g^{opt} – optical band gap calculated from UV/vis absorption spectra band edge. E_{HOMO}^{CV} – energy of highest occupied molecular orbital calculated from CV data. E_{LUMO}^{CV} – energy of lowest unoccupied molecular orbital calculated from CV data. E_g^{CV} – optical band gap calculated from CV data.

Electrochemistry

The redox properties were examined both as DCM solutions, and as films that were drop-cast deposited onto the platinum working electrode with a 0.1 M $TBAPF_6$ in propylene carbonate electrolyte solution (Fig. 2). HOMO and LUMO energy levels were determined from oxidation and reduction onsets of the thin-film measurements relative to ferrocene/ferrocenium reference using the following equation: $E_{MO} = -(4.8 + E_{onset})$ eV.[30] In solution (Fig. S15, ESI†), the HOMO energy levels for the series differ between systems, despite the lack of difference in optical bandgap, resulting in vastly different electrochemical bandgaps. However, the energies of **3–6** and **7–8** differ very little in the solid state, as seen in Fig. 3, that does agree with the optical data.

As expected, functionalization with electron deficient vinylphthalimide moieties in compounds **3** and **7** result in lower LUMO levels compared to the other derivatives flanked with electron donating thiophene groups. For compounds **3**, **5**, and **6**, the electrochemical bandgaps trend with the optical bandgaps. Compound **4** also has a decreased LUMO value, that makes the electrochemical bandgap disagree with the

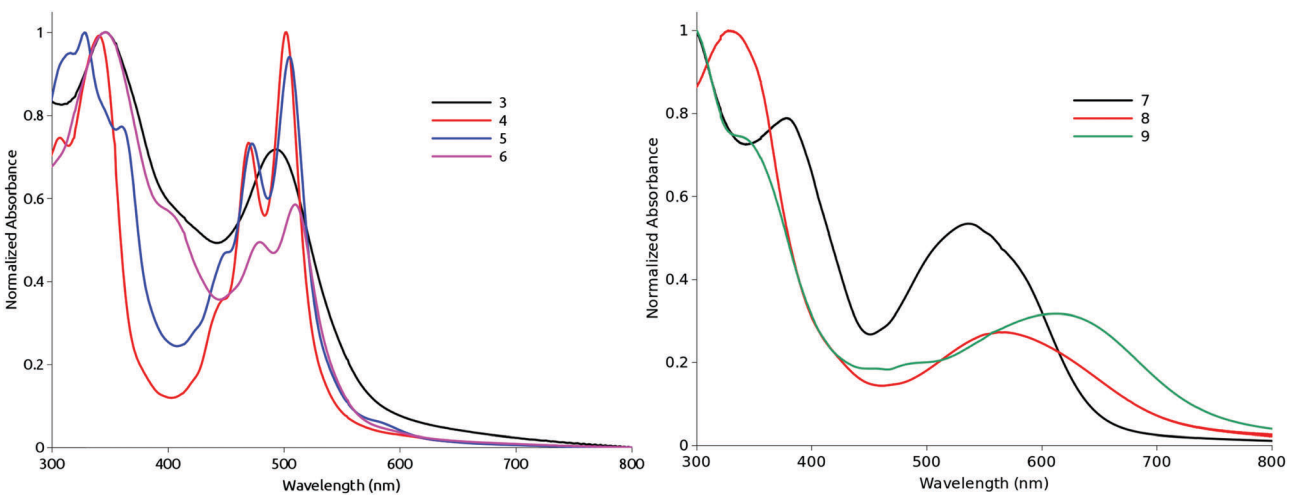

Fig. 2 Normalized film absorbance spectra of **3–6** (left), and **7–9** (right).

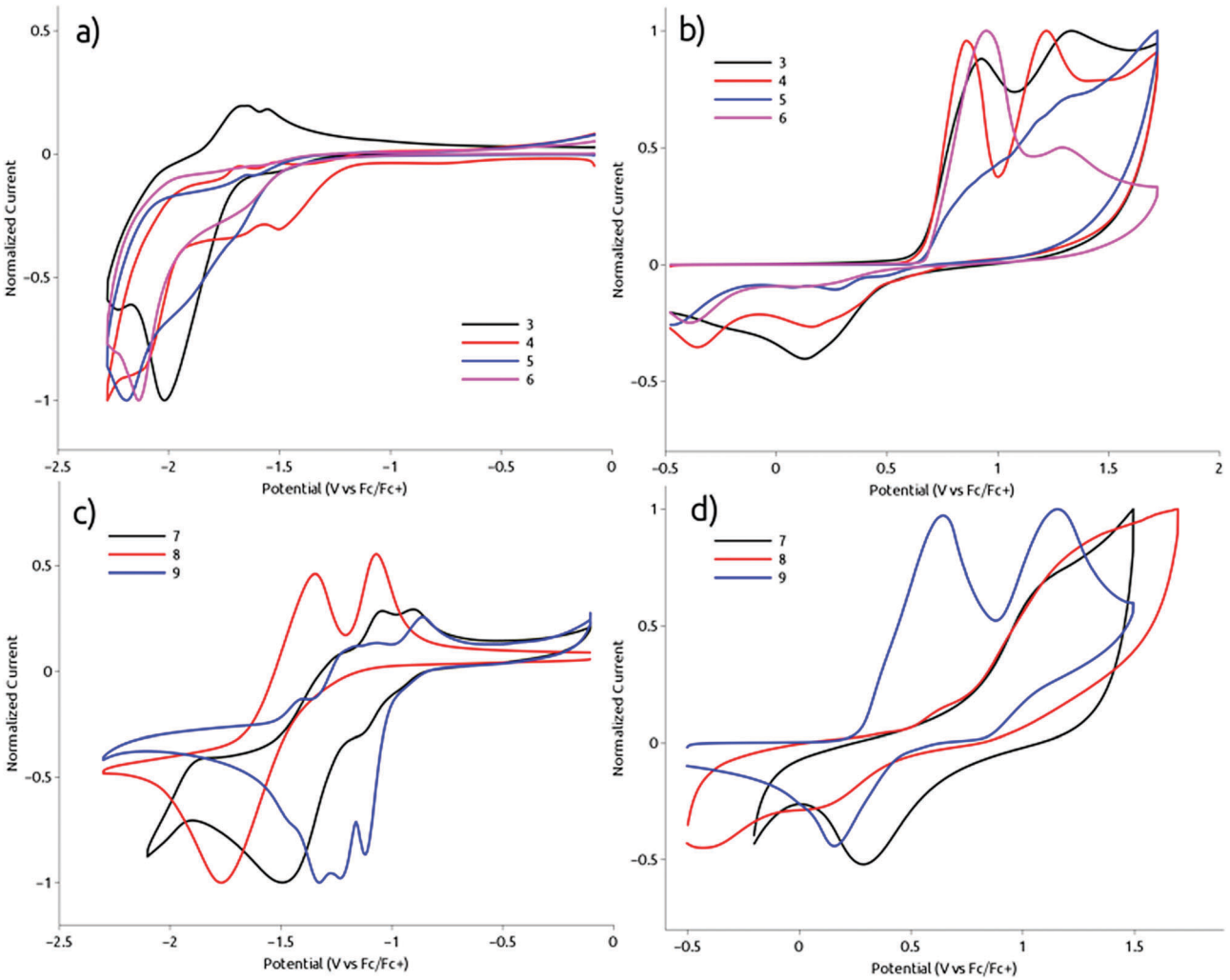

Fig. 3 Cyclic voltammetry results. (a) Reduction and (b) oxidation curves for **3–6**, (c) reduction and (d) oxidation curves for **7–9**, prepared as dropcast films.

optical bandgap. The reduction voltammogram trace has a second peak with an onset close to −1.5 V (*vs.* F_c/F_c^+) that would give it a LUMO energy level close to the other thiophene derivatives.

With the exception of **9**, the solid-state electrochemical behavior, similar to the optical behavior, is dominated by the electronics of the core, and the 6,10-groups appear to have little effect. In contrast to the optical behavior, there is significant difference in electrochemical behavior when moving to the solution state, where potential onsets differ, but do not trend with the redox potentials of the pendant groups.

The presence of the lower onset in **4** is unusual and could be a result of electrochemical instability from the unfunctionalized 5-position on thiophene. The difference in electrochemical properties is unlikely given the computational results presented in the next section.

Computational results

DFT computations of ground-state geometries and energies, and TDDFT computations of vertical excitation energies were carried out using NWChem[31] and performed using B3LYP/6-31G** for ground state computations and are shown in Fig. 4. TDDFT computations were repeated using the range-separated hybrid (RSH) functional CAM-B3LYP, that has been reported to more accurately predict excited-state and excitonic phenomena in acenes.[32] Further molecular orbital densities for all compounds in this study are provided in Fig. S17 (ESI†). Alkyl chains were approximated with methyl groups, and energy level values were taken from the calculated Kohn–Sham orbital values. Optical bandgaps were taken as the vertical excitation energies from TDDFT. Molecular orbital density surfaces were generated by Avogadro[33,34] using the POV-ray export option. As compound **4** is very similar to **5** it has been omitted from Table 2 and Fig. 4.

As seen in Table 2, there is little difference in the HOMO and LUMO levels of **5** & **6**. The resulting geometries and orbital mappings reflect this, where the attached conjugated units are nearly orthogonal to the core, and the HOMO/LUMO density is mostly contained in the core. The exception is compound **3**, where the vinylphthalimide groups are planar to the core and as a result share more density than the other compounds and

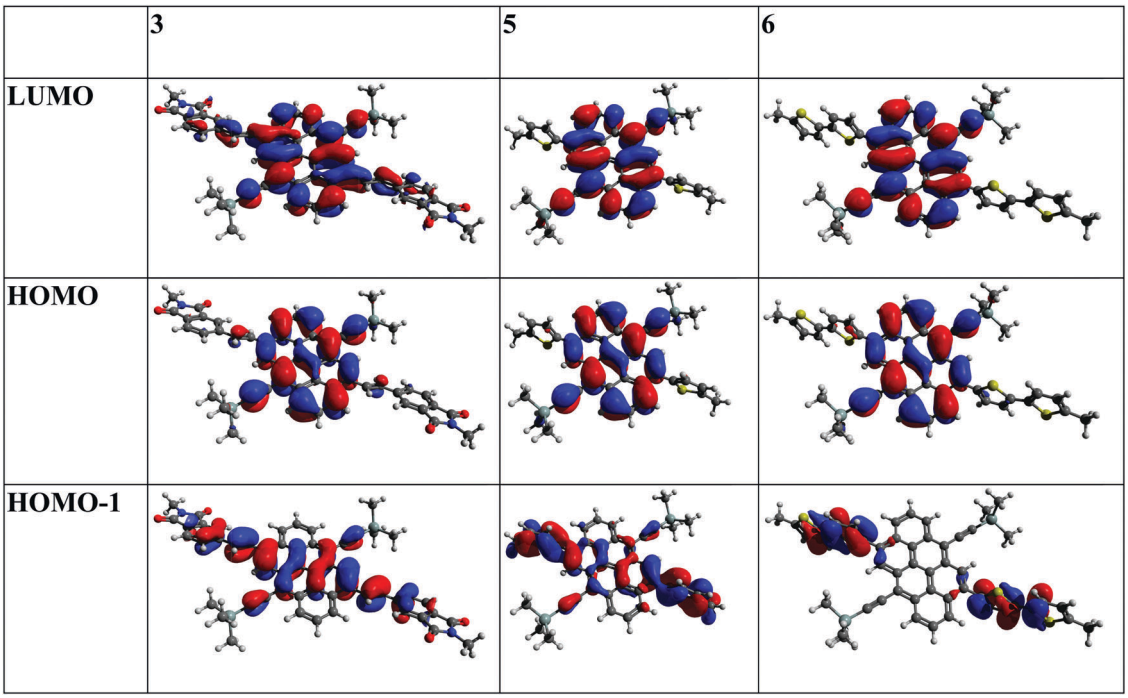

Fig. 4 Molecular orbital densities for the model compounds **3**, **5** and **6**.

Table 2 DFT computed molecular orbital energies and optical bandgaps

Compound	E_{HOMO-1} (eV)	E_{HOMO} (eV)	E_{LUMO} (eV)	E_g (eV)
3	−5.91	−5.10	−2.78	2.35
5	−5.92	−4.86	−2.41	2.57
6	−5.31	−4.90	−2.46	2.45
7	−6.56	−5.95	−3.40	2.55
8	−5.48	−5.24	−3.06	2.18
9	−4.77	−4.69	−2.79	1.63

contribute more mixing, resulting in more perturbed energy values. TDDFT data supports this conclusion, showing transitions involving the core are most favored, and transitions from pendants to core are unfavored. These correlate with the UV-Vis data, where there is little change in the bandgaps between the systems, except for **3**, where the bandgap is slightly larger.

However, this does not correlate with the solution-state electrochemistry (Fig. S15, ESI†), where the oxidation potential for each system differs depending on the conjugated units attached. This is not likely a solid-state packing effect, due in part to the lack of change in optical bandgap between the solid and solution state. This is also mirrored in the crystal structure, that still shows the thiophene rings remain orthogonal, even in the solid state. A possible explanation is the deeper molecular orbitals are oxidatively active, whereas the core can only be reduced. This correlates with the HOMO−1 orbitals for the series, that computationally show more density associated with the conjugated units attached and much larger variation in energy levels. This seems to suggest that attaching conjugated units without vinyl spacers at the 4- and 10-positions of DBC core does little to change the frontier orbital levels or the electronic and optical properties.

Single-crystal X-ray structure characterization

We attempted to prepare single crystals of the new DBC and DBC-DO derivatives using various conditions but only compounds **3** and **4** afforded crystals of sufficient size by slow evaporation from toluene, as seen in Fig. 5. The structures are centrosymmetric (**3**: $P\bar{1}$, and **4**: $P2_1/c$) with the middle of each DBC chromophore located on a center of inversion. The non-hydrogen atoms were refined with anisotropic displacement parameters. The majority of hydrogen atoms were found in difference Fourier maps, but some belonging to disordered groups had to be inferred. All hydrogens were subsequently placed at calculated positions and refined using an appropriate riding model. (Cambridge Crystallographic Data Centre, deposition numbers 1526927 (**3**) and 1526928 (**4**).†) The ellipsoid plot of **3** as shown in Fig. 6a, shows a symmetric structure, with two triisopropylsilyl groups connected to C1 and the two vinyl bridges substituted at the C4 carbon. The molecule displayed a planar core with the vinylphthalimide aromatic moieties almost in plane with the DBC due to the bridging vinyl groups. This allows close π–π stacking of the DBC cores with adjacent phthalimide moieties (Fig. 6b) to form highly inclined 1-D columnar stacks parallel to the a-axis, in which the chrysene core of one molecule π-stack with the phthalimide moiety of a translation-related $(x-1, y, z)$ molecule. The interplanar spacing between mean planes within the stacks is 3.422(4) Å.

Although crystals of **4** were produced, they were far too small for even a rotating-anode based conventional diffractometer, so data were collected on beamline 11.3.1 at the Advanced Light Source, LBNL, Berkeley, CA. The disorder in **4** consists of a ~180° flip for the thiophene group and multiple conformations for two of the isopropyl groups. These multiple conformations

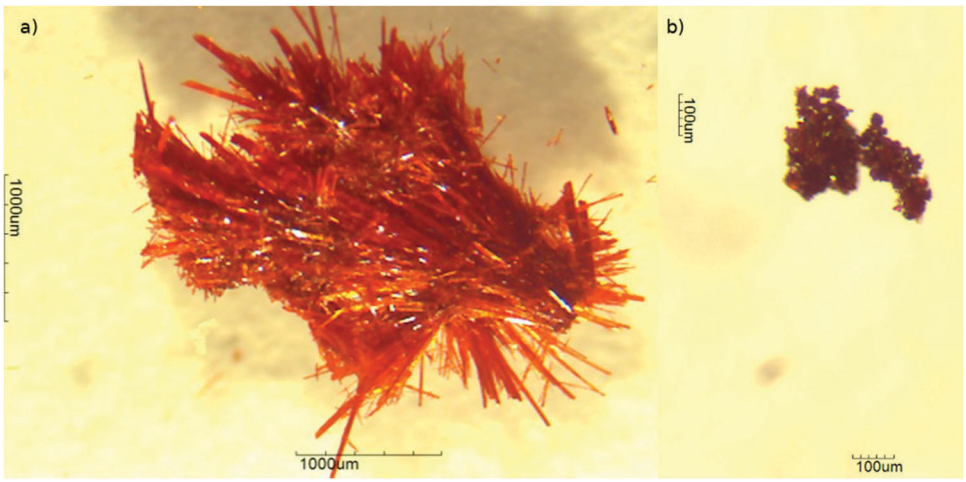

Fig. 5 Optical microscope image of crystals (a) **3** and (b) **4** under 25× magnification. Size calibration was performed against the standard given by the Moticam 10 software.

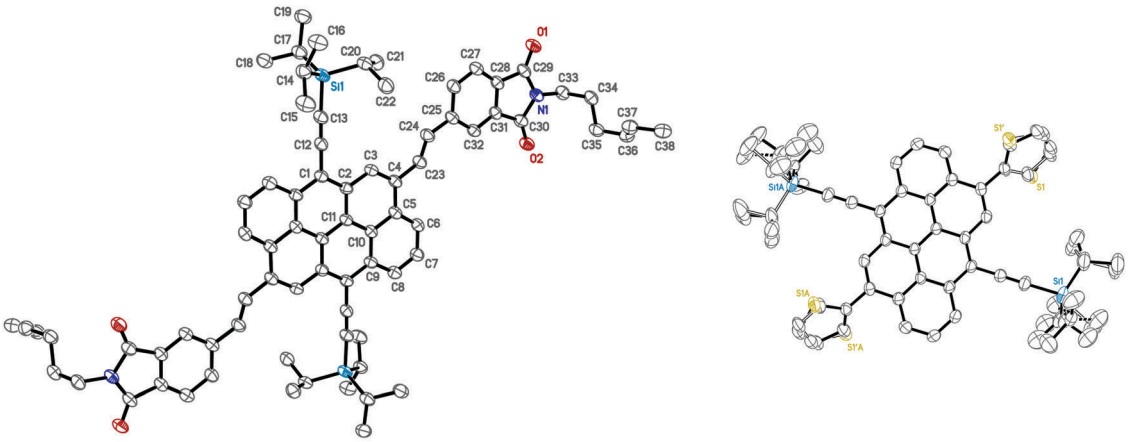

Fig. 6 Single-crystal ellipsoid plots for (a) **3** and (b) **4**. Additional plots of multiple crystals for **3** and **4** can be found in Fig. S19–S24 (ESI†).

in the crystal structures could possibly be the cause of the multiple melting peaks in the DSC traces for the thiophene compounds **4–6** (Fig. S11, ESI†). In **4**, molecules pack in a herringbone motif with two different C–H$\cdots\pi$ interactions as the principal contacts between aromatic groups. In the first such interaction, the C7–H7 bond is directed towards a screw-related $(1 - x, 0.5 + y, 1.5 - z)$ thiophene. The second interaction is complicated by disorder of the thiophene. For the major component of disorder, the C25–H25 thiophene bond is directed toward the chrysene core of a glide-related $(x, 1.5 - y, 0.5 + z)$ molecule. Additional packing plots for **3** and **4** can be found in Fig. S19–S24 (ESI†).

Conclusion

Starting from an inexpensive textile dye, 4,10-dibromo-dibenzo-[def,mno] chrysene-6,12-dione (Vat Orange #3), we have described the synthesis and purification of a variety of novel substituted dibenzo[def,mno]chrysene (DBC) and dibenzo[def,mno]chrysene-6,12-dione (DBC-DO) based derivatives. We have characterized all the compounds using UV-Vis, CV, NMR, MALDI, X-ray, and computational analysis. Initial observations for the thiophene substituted compounds suggest that the optoelectronic behavior is dominated by the DBC and DBC-DO cores. This results from the near orthogonal orientation of the thiophene rings to the cores. Only with the vinylphthalimide substituted cores do we observe orbital overlap between the core and substituent due to the planarity of the system, as determined both computationally and experimentally. Crystal structures show the favorable π–π stacking of the DBC core, forming columnar stacking arrangements in **3** favorable for semiconductor applications. Future work will include fabrication of organic photovoltaics (OPV) and thin-film transistors (OTFT) from selected materials in this study.

General experimental and characterization methods

All reagents and solvents were purchased from commercial vendors unless otherwise noted. The starting compound **1** was purchased from BOC Sciences. ^{1}H and ^{13}C NMR spectra were obtained on a JEOL ECA 500 liquid-state NMR spectrometer

and data obtained was manipulated in ACD/NMR processor software.

X-ray data were collected on either a Bruker-Nonius X8 Proteum CCD diffractometer using CuKα radiation, or at the ALS synchrotron, beamline 11.3.1 (BNL, Berkeley). Raw diffraction frames were integrated, scaled, merged and corrected for Lorentz-polarization effects using the APEX2 package.[35] The structures were solved using SHELXT[36] and refined using SHELXL-2014.[37] Molecule editing, including the construction of a suitable disorder model for **4** was performed using the XP program of the SHELXTL package.[38] Hydrogen atoms were included using a riding model. The final models were checked using an *R*-tensor,[39] and by validation routines of the Platon program[40] as implemented in the IUCr checkCIF facility.

Mass spectrometric measurements were acquired in positive-ion and negative-ion modes with a Bruker Ultraflextreme MALDI-TOF mass spectrometer (Bruker Daltonics, Billerica, MA) equipped with a 355 nm Nd:YAG laser. Spectra were collected in reflector mode with a grid voltage of 50.3%, and a low mass cutoff of 200 Da. Five replicate spectra were collected for each analysis as 100 shot composites at a sampling frequency of 1 kHz using automated laser rastering.

UV-Vis spectra were obtained using a Beckman-Coulter DU800 spectrophotometer, using quartz 1 cm pathlength cells for solution phase, and microscope coverslips for film measurements.

Cyclic voltammetry was performed in a three-electrode electrochemical cell with a platinum wire as the counter electrode, Ag/Ag^+ wire as the reference electrode, and a platinum disk (0.02 cm^2) as the working electrode with a Princeton Applied Research Versa STAT 3 potentiometer. Film measurements were performed by drop casting films onto the working electrode from 1 mg/1 mL solution of the sample in chloroform. Measurements were performed in 0.1 M tetrabutylammonium hexafluorophosphate electrolyte in propylene carbonate solution (purged with argon) using a scan rate of 50 mV s^{-1}. Solution phase measurements were performed in dichloromethane with the same electrolyte and concentration.

Experimental section

((4,10-Dibromo-6,12-dihydronaphtho[7,8,1,2,3-nopqr]-tetraphene-6,12-diyl)bis(ethyne-2,1-diyl))-bis(triisopropylsilane)[22] (2)

To a solution of (triisopropylsilyl)acetylene (4.48 mL, 20 mmol) in anhydrous THF (120 mL) was added *n*-BuLi (2 M in cyclohexane, 9.2 mL, 18.4 mmol) dropwise over 10 min at −78 °C under nitrogen atmosphere. The clear solution was further stirred for 1 h at 0 °C when 4,10-dibromoanthanthrone (**1**) (1.002 g, 2.16 mmol) was added in one portion turning the color of the solution into a dark red color. The reaction was allowed to warm up to room temperature and was stirred overnight. Then a solution of 3 M HCl (12 mL) containing $SnCl_2{\cdot}2H_2O$ (3.61 g, 16 mmol) was added dropwise at 0 °C changing the color of the reaction from orange to red. Then the reaction was allowed to warm up to room temperature and stirred for 3 h followed by pouring into 200 mL of water. And then it was poured into 200 mL of water. The organic layer was extracted with chloroform and dried over $MgSO_4$. The crude product was purified by a short silica gel column by eluting with DCM : hexanes (1 : 1) affording compound **2** (1.40 g, 81.5%) of an orange solid. ^{1}H NMR (500 MHz, $CDCl_3$): δ 9.11 (d, 4H, J = 5 Hz), 8.73 (s, 2H), 8.30 (d, 2H, J = 10 Hz), 1.12–1.56 (m, 42H).

5,5′-((1*E*,1′*E*)-(6,12-Bis((triisopropylsilyl)ethynyl)naphtho[7,8,1,2,3-nopqr]-tetraphene-4,10-diyl)bis(ethene-2,1-diyl))bis(2-hexylisoindoline-1,3-dione) (3)

A 100 mL round bottom flask was charged with compound **2** (0.398 g, 0.5 mmol), 2-hexyl-5-vinylisoindoline-1,3-dione (0.335 g, 1.3 mmol), $Pd(P(t\text{-}Bu)_3)_2$ (0.013 g, 0.025 mmol) and purged with argon. Then, toluene (20 mL) was added and the mixture was stirred at room temperature resulting in a homogenous brown-orange solution. After adding *N*,*N*-dicyclohexylmethylamine (0.214 mL, 1 mmol), the reaction mixture was heated at 100 °C for 24 h. Then, the reaction was cooled down to room temperature when it was quenched with aqueous 2 M HCl. The product was extracted with DCM and the combined organic layers were washed with water. After drying over $MgSO_4$, the solvent was evaporated yielding crude product as a solid. The title compound was purified over silica gel column chromatography eluting with hexanes : DCM (6 : 4) affording 0.340 g (59.3%) of a yellow-brown powder. ^{1}H NMR (500 MHz, $CDCl_3$): δ 9.24 (d, 2H, J = 10 Hz), 9.17 (s, 2H), 8.66 (d, 2H, J = 5 Hz), 8.35 (m, 2H), 8.23 (s, 2H), 7.92 (s, 4H), 7.62 (d, 2H, J = 10 Hz), 3.75 (t, 4H, J = 10 Hz), 1.69–1.79 (m, 4H), 1.22–1.48 (m, 54H), 0.92 (t, 6H, J = 14 Hz). MALDI-TOF: $C_{76}H_{86}N_2O_4Si_2$ (calc. 1146.61) found 1147.64[M^+] m/z.

((4,10-Di(thiophen-2-yl)naphtho[7,8,1,2,3-nopqr]tetraphene-6,12-diyl)bis(ethyne-2,1-diyl))bis(triisopropylsilane) (4)

A 100 mL round bottom flask was charged with compound **2** (0.398 g, 0.5 mmol), thiophen-2-ylboronic acid (0.384 g, 3 mmol), a spatula tip of Aliquat 336, $Pd(PPh_3)_4$ (0.023 g, 0.02 mmol), toluene (20 mL) and degassed with nitrogen. After adding 2 M K_2CO_3 (5 mL) in water, the reaction mixture was heated at 100 °C for 48 h. Then, the reaction was cooled down to room temperature when it was quenched with aqueous 2 M HCl. The product was extracted with DCM and the combined organic layers were washed with water. After drying over $MgSO_4$, the solvent was evaporated yielding crude product as a solid. It was purified over silica gel column chromatography eluting with chloroform affording the title compound (0.236 g, 58.9%) of a red solid. ^{1}H NMR (500 MHz, $CDCl_3$): δ 9.21 (d, 2H, J = 5 Hz), 9.00 (s, 2H), 8.80 (d, 2H, J = 5 Hz), 8.27 (t, 2H, J = 10 Hz), 7.60 (d, 2H, J = 5 Hz), 7.57 (d, 2H, J = 5 Hz), 7.33 (dd, 2H, J = 5.2 Hz, J = 3.4), 1.18–1.42 (m, 42H). MALDI-TOF: $C_{52}H_{56}S_2Si_2$ (calc. 800.34) found 800.99 [M^+] m/z.

((4,10-Bis(5-hexylthiophen-2-yl)naphtho[7,8,1,2,3-nopqr]-tetraphene-6,12-diyl)bis(ethyne-2,1-diyl))bis(triisopropylsilane) (5)

A 100 mL round bottom flask was charged with compound **2** (0.302 g, 0.38 mmol), tributyl(5-hexylthiophen-2-yl)stannane

(0.695 g, 1.52 mmol), $Pd(PPh_3)_4$ (0.022 g, 0.02 mmol), toluene (20 mL) and degassed with nitrogen. Then, the reaction mixture was heated at 100 °C for 48 h. After, the reaction was cooled down to room temperature, it was quenched with aqueous 2 M HCl. The product was extracted with DCM and the combined organic layers were washed with water. After drying over $MgSO_4$, the solvent was evaporated yielding crude product as a solid. It was purified over silica gel column chromatography eluting with chloroform affording the title compound (0.277 g, 75.2%) of a red solid. ^{1}H NMR (500 MHz, $CDCl_3$): δ 9.21 (d, 2H, J = 5 Hz), 8.97 (s, 2H), 8.87 (d, 2H, J = 5 Hz), 8.26 (t, 2H, J = 10 Hz), 7.41 (d, 2H, J = 5 Hz), 6.98 (d, 2H, J = 5 Hz), 2.98 (t, 4H, J = 10 Hz), 1.81–1.87 (m, 4H), 1.30–1.45 (m, 54H), 0.96 (t, 6H, J = 14 Hz). MALDI-TOF: $C_{64}H_{80}S_2Si_2$ (calc. 968.52) found 968.66 [M^+] m/z.

((4,10-Bis(5′-hexyl-[2,2′-bithiophen]-5-yl)naphtho[7,8,1,2,3-nopqr]tetraphene-6,12-diyl)bis(ethyne-2,1-diyl))-bis(triisopropylsilane) (6)

A 100 mL round bottom flask was charged with compound 2 (0.151 g, 0.19 mmol), 2-(5-hexylthiophen-2-yl)-4,4,5,5-tetramethyl-1,3,2-dioxaborolane (0.226 g, 0.6 mmol), a spatula tip of Aliquat 336, $Pd(PPh_3)_4$ (0.011 g, 0.01 mmol), toluene (20 mL) and degassed with nitrogen. After adding aqueous 2 M K_2CO_3 (5 mL), the reaction mixture was heated at 100 °C for 48 h. Then, the reaction was cooled down to room temperature when it was quenched with aqueous 2 M HCl. The product was extracted with DCM and the combined organic layers were washed with water. After drying over $MgSO_4$, the solvent was evaporated yielding crude product as a solid. It was purified over silica gel column chromatography eluting with chloroform affording the title compound (0.138 g, 64.2%) of a red solid. ^{1}H NMR (500 MHz, $CDCl_3$): δ 9.21 (d, 2H, J = 10 Hz), 9.02 (s, 2H), 8.89 (d, 2H, J = 5 Hz), 8.28 (t, 2H, J = 10 Hz), 7.51 (d, 2H, J = 5 Hz), 7.30 (d, 2H, J = 5 Hz), 7.13 (d, 2H, J = 5 Hz), 6.77 (d, 2H, J = 5 Hz), 2.87 (t, 4H, J = 10 Hz), 1.70–1.80 (m, 4H), 1.20–1.54 (m, 54H), 0.93 (t, 6H, J = 5 Hz). MALDI-TOF: $C_{72}H_{84}S_4Si_2$ (calc. 1132.50) found 1135.32 [M^+] m/z.

1-Bromo-2-octyldodecane

2-Octyldodecanol (2.86 mL, 8 mmol), was added to a dry round-bottom flask and dissolved in DCM (35 mL). Triphenylphosphine (2.93 g, 11.2 mmol) was added in one portion and the reaction cooled to 0 °C. *N*-Bromosuccinimide (1.85 g, 10.1 mmol) was added slowly over the course of 30 minutes. The reaction mixture was allowed to warm to room temperature and stirred for 24 hours. The solvent was removed from the crude reaction by rotary evaporation, and the product extracted by trituration with hexanes. The hexanes solution was reduced in volume under vacuum and purified by flash chromatography to yield a clear viscous oil (2.8 g, 99%).

4-Bromophthalimide

4-Bromophthalic anhydride (1.0 g, 4.4 mmol), ammonium acetate (0.67 g, 8.8 mmol), and 4-(*N*,*N*-dimethylamino)pyridine (53 mg, 0.44 mmol) were placed in a dry microwave vessel and heated at 150 °C for 5 min. The crude solid was suspended in deionized water, filtered and washed with excess water, yielding a crystalline white solid (0.65 g, 66%). ^{1}H NMR (500 MHz, DMSO-d_6): δ 11.36 (br s, 1H), 7.97 (m, 2H), 7.71 (dd, 1H, J = 0.60, 7.82).

4-Bromo-*N*-(2-octyldodecyl)phthalimide

4-Bromophthalimide (0.44 g, 2.0 mmol), and K_2CO_3 (0.51 g, 3.7 mmol) were added to a dry Schlenk flask, then flushed with inert gas. Dry DMF (15 mL) was added, and the reaction heated at 100 °C for 1 h. 2-Octyldodecanol (0.71 g, 2.0 mmol) was added in one portion, and the reaction held at 100 °C overnight. The crude mixture was poured into excess water, extracted with ethyl acetate, the organic portions collected and dried with $MgSO_4$, filtered, and the filtrate reduced in volume under vacuum. The crude solid was purified by flash chromatography to yield a yellow oil (0.53 g, 55%). ^{1}H NMR (500 MHz, $CDCl_3$): δ 7.69 (d, 1H, J = 1.60 Hz), 7.83 (dd, 1H, J = 1.60, 7.88 Hz), 7.69 (d, 1H, J = 7.90 Hz), 3.55 (d, 2H, J = 7.25 Hz), 1.86 (m, 1H), 1.23 (m, 32H), 0.87 (m, 6H).

4-Ethenyl-*N*-(2-octyldodecyl)phthalimide

4-Bromo-*N*-(2-octyldodecyl)phthalimide (0.5 g, 1.0 mmol), potassium trifluorovinylborate (0.16 g, 1.18 mmol), triphenylphosphine (16 mg, 60 μmol), palladium(II) acetate (4.5 mg, 20 μmol), Cs_2CO_3 (0.96 g, 2.9 mmol) were added to a dry Schlenk flask and de-gassed by vacuum and backfilling with inert gas three times. THF : H_2O (9 : 1, 10 mL) was added, and the reaction heated at 55 °C overnight. The reaction was then poured into excess water, extracted with ethyl acetate, the organic portions collected and dried with $MgSO_4$, filtered, and the filtrate reduced in volume under vacuum. The crude solid was purified by flash chromatography to yield a viscous yellow oil (0.26 g, 59%). ^{1}H NMR (500 MHz, $CDCl_3$): δ 7.87 (d, 1H, J = 1.40 Hz), 7.76 (d, 1H, J = 7.70 Hz), 7.66 (dd, 1H, J = 1.40, 7.72 Hz), 6.80 (dd, 1H, J = 10.95, 17.55 Hz), 5.94 (d, 1H, J = 17.55 Hz), 5.47 (d, 1H, J = 10.90), 3.55 (d, 2H, J = 7.25 Hz), 1.86 (m, 1H), 1.22 (m, 32H), 0.86 (m, 6H).

N,*N*-Di(4-methoxyphenyl)-4-(4,4,5,5-tetramethyl-1,3,2-dioxaborolan-2-yl)benzamine

N,*N*-Di(4-methoxyphenyl)-4-iodobenzamine (0.5 g, 1.2 mmol), bis(pinacolato)diboron (0.37 g, 1.4 mmol), palladium(II) bis(diphenylphosphino)ferrocene dichloride (35 mg, 0.048 mmol), and potassium acetate (0.28 g, 2.88 mmol) were placed in a dry Schlenk flask and de-gassed by vacuum and back-filling with inert gas three times. DMSO (15 mL) was added and the reaction was heated at 100 °C overnight. The reaction was then poured into excess water, extracted with ethyl acetate, the organic portions collected and dried with $MgSO_4$, filtered, and the filtrate reduced in volume under vacuum. The crude solid was purified by flash chromatography to yield a greasy yellow solid (0.28 g, 55%). ^{1}H NMR (500 MHz, $CDCl_3$): δ 7.58 (m, 2H), 7.04 (m, 4H), 6.83 (m, 6H), 3.79 (s, 6H), 1.25 (s, 12H).

4,10-Bis(4-ethenyl-*N*-[2-octyldodecyl]phthalimide)-anthanthrone (7)

1 (0.10 g, 0.22 mmol), 4-ethenyl-*N*-(2-octyldodecyl)phthalimide (0.25 g, 0.55 mmol), *N*,*N*-dicyclohexylmethylamine (0.22 mL, 0.44 mmol), and bis(tri-*t*-butylphosphine)palladium (5.6 mg,

11 μmol) were placed in a dry Schlenk flask and de-gassed with vacuum and back-filling with inert gas, three times. Toluene (5 mL) was added and the reaction heated at 80 °C for 3 days. The reaction was then poured into excess 5% HCl in MeOH (v/v) and collected by filtration. This solid was then suspended in DCM and filtered, and the filtrate concentrated to yield a brick-red powder (56 mg, 21%). ^{1}H NMR (500 MHz, $CDCl_3$): δ 8.86 (d, 2H, J = 8.00 Hz), 8.82 (s, 2H), 8.68 (d, 2H, J = 8.25 Hz), 8.21 (s, 2H), 8.16 (d, 2H, J = 16.00 Hz), 7.99 (t, 2H, J = 7.80 Hz), 7.92 (s, 4H), 7.60 (d, 2H, J = 16.05 Hz), 3.64 (d, 4H, J = 7.30 Hz), 1.91 (m, 2H), 1.37 (m, 4H), 1.27 (m, 64H), 0.89 (t, 12H, J = 14 Hz). MALDI-TOF: $C_{82}H_{100}N_2O_6$ (calc. 1209.68) found 1210.67 [M^-] m/z.

4,10-Bis(5-hexylbithiophen-2′-yl)anthanthrone (8)

1 (0.30 g, 0.64 mmol), 2′-(5-hexylbithiophen-2′-yl)-4,4,5,5-tetramethyl-1,3,2-dioxaborolane (0.73 g, 1.93 mmol), cesium fluoride (0.29 g, 1.93 mmol), and bis(tri-*t*-butylphosphine)-palladium (5.6 mg, 11 μmol) were placed in a dry Schlenk flask and de-gassed with vacuum and back-filling with inert gas, three times. THF : H_2O (15 mL, 15 : 1) was added and the reaction heated at 55 °C overnight. The crude mixture was absorbed directly onto silica and purified by flash chromatography using a hexanes to DCM gradient to yield a dark purple powder (80 mg, 15%). ^{1}H NMR (500 MHz, $CDCl_3$): δ 8.84 (d, 2H, J = 8.05 Hz), 8.78 (d, 2H, J = 6.50 Hz), 8.52 (s, 2H), 7.93 (m, 2H), 7.30 (m, 2H), 7.10 (m, 2H), 6.74 (m, 2H), 2.83 (t, 4H, J = 7.00 Hz), 1.72 (m, 4H), 1.42 (m, 4H), 1.33 (m, 8H), 0.91 (t, 6H, J = 5.05 Hz). MALDI-TOF: $C_{50}H_{42}O_2S_4$ (calc. 802.21) found 802.62 [M^-] m/z.

4,10-Bis(*N*,*N*-di(4-methoxyphenyl)benzamino-4-yl)-anthanthrone (9)

1 (90 mg, 0.19 mmol), *N*,*N*-di(4-methoxyphenyl)-4-(4,4,5,5-tetramethyl-1,3,2-dioxaborolan-2-yl)benzamine (0.25 g, 0.57 mmol), cesium fluoride (88 mg, 0.58 mmol), and bis(tri-*t*-butylphosphine)-palladium (5.6 mg, 11 μmol) were placed in a dry Schlenk flask and de-gassed with vacuum and back-filling with inert gas, three times. THF : H_2O (7 mL, 15 : 1) was added and the reaction heated at 55 °C overnight. The reaction was then poured into excess 5% HCl in MeOH (v/v) and collected by filtration. This solid was then suspended in DCM and filtered, and the filtrate concentrated to yield a blue-black powder (68 mg, 39%). ^{1}H NMR (500 MHz, $CDCl_3$): δ 8.65 (d, 2H, J = 7.20 Hz), 8.45 (d, 2H, J = 8.30), 8.35 (s, 2H), 7.79 (m, 2H), 7.39 (d, 4H, J = 8.55 Hz), 7.18 (d, 8H, J = 8.85 Hz), 7.08 (d, 4H, J = 8.55 Hz), 6.89 (d, 8H, J = 8.85), 3.82 (s, 12H). MALDI-TOF: $C_{62}H_{44}N_2O_6$ (calc. 913.02) found 914.12 [MH^+] m/z.

Acknowledgements

This work was partially supported by funds provided by the Global Climate and Energy Project (GCEP) award # 1138721 and by the Center for Advanced Molecular Photovoltaics (CAMP), award # KUS-C1-015-21 made by the King Abdullah University of Science and Technology (KAUST). Funding was also provided by the Research Corporation for Science Advancement (RCSA) through the Scialog Collaborative Innovation Award (#22355), and start up funds from the Colorado School of Mines (AS). We thank Prof. Alberto Salleo and Ms Camila Arantxa Cendra Guinassi from Stanford University, Department of Materials Science and Engineering for their help in testing these materials in organic field-effect transistors (OFETs). The Advanced Light Source is supported by the Director, Office of Science, Office of Basic Energy Sciences of the U.S. Department of Energy under Contract No. DE-AC02-05CH11231. Crystallographic data for the structures reported in this paper have been deposited with the CCDC 1526927 and 1526928.†

References

1 A. C. Arias, J. D. MacKenzie, I. McCulloch, J. Rivnay and A. Salleo, *Chem. Rev.*, 2010, **110**, 3–24.
2 C. D. Dimitrakopoulos and P. R. L. Malenfant, *Adv. Mater.*, 2002, **14**, 99–117.
3 A. C. Grimsdale, K. L. Chan, R. E. Martin, P. G. Jokisz and A. B. Holmes, *Chem. Rev.*, 2009, **109**, 897–1091.
4 A. Pron, P. Gawrys, M. Zagorska, D. Djurado and R. Demadrille, *Chem. Soc. Rev.*, 2010, **39**, 2577–2632.
5 J. Roncali, *Chem. Rev.*, 1997, **97**, 173–205.
6 B. Walker, C. Kim and T. Q. Nguyen, *Chem. Mater.*, 2011, **23**, 470–482.
7 S. Kazim, F. J. Ramos, P. Gao, M. K. Nazeeruddin, M. Gratzel and S. Ahmad, *Energy Environ. Sci.*, 2015, **8**, 1816–1823.
8 H. Minemawari, T. Yamada, H. Matsui, J. Tsutsumi, S. Haas, R. Chiba, R. Kumai and T. Hasegawa, *Nature*, 2011, **475**, 364–367.
9 J. E. Anthony, *Angew. Chem., Int. Ed.*, 2008, **47**, 452–483.
10 B. Lucas, T. Trigaud and C. Videlot-Ackermann, *Polym. Int.*, 2012, **61**, 374–389.
11 A. Ciesielski, D. K. Stepien, M. A. Dobrowolski, L. Dobrzycki and M. K. Cyranski, *Chem. Commun.*, 2012, **48**, 10129–10131.
12 P. V. Schleyer, M. Manoharan, H. J. Jiao and F. Stahl, *Org. Lett.*, 2001, **3**, 3643–3646.
13 M. Linares, D. Beljonne, J. Cornil, K. Lancaster, J. L. Bredas, S. Verlaak, A. Mityashin, P. Heremans, A. Fuchs, C. Lennartz, J. Ide, R. Mereau, P. Aurel, L. Ducasse and F. Castet, *J. Phys. Chem. C*, 2010, **114**, 3215–3224.
14 M. Bendikov, F. Wudl and D. F. Perepichka, *Chem. Rev.*, 2004, **104**, 4891–4945.
15 Y. Cao, Y. Liang, L. Zhang, S. Osuna, A. L. M. Hoyt, A. L. Briseno and K. N. Houk, *J. Am. Chem. Soc.*, 2014, **136**, 10743–10751.
16 L. Zhang, Y. Cao, N. S. Colella, Y. Liang, J. L. Bredas, K. N. Houk and A. L. Briseno, *Acc. Chem. Res.*, 2015, **48**, 500–509.
17 K. B. Burke, Y. Shu, P. Kemppinen, B. Singh, M. Bown, I. I. Liaw, R. M. Williamson, L. Thomsen, P. Dastoor, W. Belcher, C. Forsyth, K. N. Winzenberg and G. E. Collis, *Cryst. Growth Des.*, 2012, **12**, 725–731.
18 R. Cardia, G. Malloci, A. Mattoni and G. Cappellini, *J. Phys. Chem. A*, 2014, **118**, 5170–5177.
19 A. N. Simonov, P. Kemppinen, C. Pozo-Gonzalo, J. F. Boas, A. Bilic, A. D. Scully, A. Attia, A. Nafady, E. A. Mashkina, K. N. Winzenberg, S. E. Watkins and A. M. Bond, *J. Phys. Chem. B*, 2014, **118**, 6839–6849.

20 K. N. Winzenberg, P. Kemppinen, G. Fanchini, M. Bown, G. E. Collis, C. M. Forsyth, K. Hegedus, T. B. Singh and S. E. Watkins, *Chem. Mater.*, 2009, **21**, 5701–5703.
21 L. Zhang, B. Walker, F. Liu, N. S. Colella, S. C. B. Mannsfeld, J. J. Watkins, T. Q. Nguyen and A. L. Briseno, *J. Mater. Chem.*, 2012, **22**, 4266–4268.
22 J. B. Giguere, J. Boismenu-Lavoie and J. F. Morin, *J. Org. Chem.*, 2014, **79**, 2404–2418.
23 J. B. Giguere and J. F. Morin, *J. Org. Chem.*, 2013, **78**, 12769–12778.
24 J. B. Giguere, Q. Verolet and J. F. Morin, *Chem. – Eur. J.*, 2013, **19**, 372–381.
25 B. K. Shah, D. C. Neckers, J. M. Shi, E. W. Forsythe and D. Morton, *J. Phys. Chem. A*, 2005, **109**, 7677–7681.
26 Y. J. Kim, J. S. Lee, J. Hong, Y. Kim, S. B. Lee, S.-K. Kwon, Y.-H. Kim and C. E. Park, *J. Polym. Sci., Part A: Polym. Chem.*, 2016, **54**, 2559–2570.
27 Y. Kim, S. B. Lee, S. H. Jang, T. K. An, S. H. Kim, Y.-H. Kim and C. E. Park, *Dyes Pigm.*, 2016, **130**, 176–182.
28 P. Sonar, M. S. Soh, Y. H. Cheng, J. T. Henssler and A. Sellinger, *Org. Lett.*, 2010, **12**, 3292–3295.
29 S. M. Ryno, C. Risko and J. L. Bredas, *J. Am. Chem. Soc.*, 2014, **136**, 6421–6427.
30 C. M. Cardona, W. Li, A. E. Kaifer, D. Stockdale and G. C. Bazan, *Adv. Mater.*, 2011, **23**, 2367–2371.
31 M. Valiev, E. J. Bylaska, N. Govind, K. Kowalski, T. P. Straatsma, H. J. J. Van Dam, D. Wang, J. Nieplocha, E. Apra, T. L. Windus and W. de Jong, *Comput. Phys. Commun.*, 2010, **181**, 1477–1489.
32 B. M. Wong and T. H. Hsieh, *J. Chem. Theory Comput.*, 2010, **6**, 3704–3712.
33 M. D. Hanwell, D. E. Curtis, D. C. Lonie, T. Vandermeersch, E. Zurek and G. R. Hutchison, *J. Cheminf.*, 2012, **4**, 1–17.
34 Avogadro: an open-source molecular builder and visualization tool.
35 *APEX-2, SAINT-Plus, SADABS.*, Bruker-AXS, Madison, WI, USA, 2008.
36 G. M. Sheldrick, *Acta Crystallogr., Sect. A: Found. Crystallogr.*, 2015, **71**, 3–8.
37 G. M. Sheldrick, *Acta Crystallogr., Sect. C: Cryst. Struct. Commun.*, 2015, **71**, 3–8.
38 G. M. Sheldrick, *Acta Crystallogr., Sect. A: Found. Crystallogr.*, 2008, **64**, 112–122.
39 S. Parkin, *Acta Crystallogr., Sect. A: Found. Crystallogr.*, 2000, **56**, 157–162.
40 A. L. Spek, *Acta Crystallogr., Sect. D: Biol. Crystallogr.*, 2009, **65**, 148–155.